# Effect of Cr Layer on the Structure and Properties of Cr/DLC Films

**Xiaohong Jiang[1], A.V. Rogachev[2], D.G. Piliptsou[2*]**

[1]Nanjing University of Science and Technology, Nanjing 210094, China,
[2]Francisk Skorina Gomel State University, Gomel 246019, Belarus

## Article info

## Abstract

This paper focuses on the Cr interlayer effect on the structure and properties of Cr/DLC films. To improve structural, mechanical and chemical properties of a-C films, we developed two layer chromium-carbon films produced by cathode magnetic filtered arc deposition. Microstructure and properties of these films are explained depending on the Cr-interlayer size. The structure is analyzed by Raman spectroscopy. Moreover, we also estimated residual stress, the friction coefficient, hardness, the elastic modulus and corrosion parameters by X-ray double crystal surface profilometry, tribotesting, nanoindenter-testing, as well as contact angle measurements and potentiodynamic polarization analysis. As a result of the comparative analysis, we revealed a substantial improvement in the characteristics of the produced two layer films. The results provide theoretical basis for the application of these films.

## 1. Introduction

Diamond-like carbon (DLC) films have being developed for a wide range of applications related to fabrication of mechanical, acoustic, electronic, and optical devices [1]. Diamond-like carbon film is composed by diamond phase ($sp^3$ carbon hybrid structure) and graphite phase ($sp^2$ carbon hybrid structure), which makes it have many excellent performance, such as high hardness, low friction coefficient, good light transmittance, stable chemical properties and good biological compatibility. DLC film is a new type of film material that can be widely used in mechanics, optics, electronics, biomedical and other fields [2]. However, in the process of research and application, the defects of DLC films like high internal stress, poor toughness and thermal stability weaken its performance and lifetime. To improve these detects, researchers have been done a series of studies and find that methods, including basal surface pretreatment, doping heterogeneous elements, using interlayer film, annealing treatment, all can improve the performance effectively [3].

There are still challenges in the deposition of carbon films with good integrated performance for engineering applications. To address these challenges, different technological methods are used such as doping of different metals or incorporating an additional layer (interlayer) of metal into the DLC films [4]. When nano-scaled metal layers are used as an element of multilayer film, however, their thickness should be expected to produce a specific structural effect, e.g. the catalytic or inhibitory effect of the metal surface on the synthesis of carbon clusters, especially for the case that presents the processes of diffusion and chemical interaction. They bring controllable improvements into some properties and performance of the treated parts. Chromium (Cr) is a carbide-forming element which interacts with carbon more active than, for example, titanium or aluminum [5]. The reaction of Cr within the carbon matrix induces some changes in the structure and properties of Cr/DLC films [6].

In the work, Cr/DLC films with different Cr thickness were fabricated by cathode arc plasma technique. The effects of thickness of the Cr-interlayer on the microstructure, mechanical properties and corrosive resistance were studied.

## 2. Experimental

DLC films with the Cr interlayer were prepared using a cathode magnetic filtered arc deposition device with double-excitation source. The scheme of vacuum chamber and appearance are shown in Fig. 1.
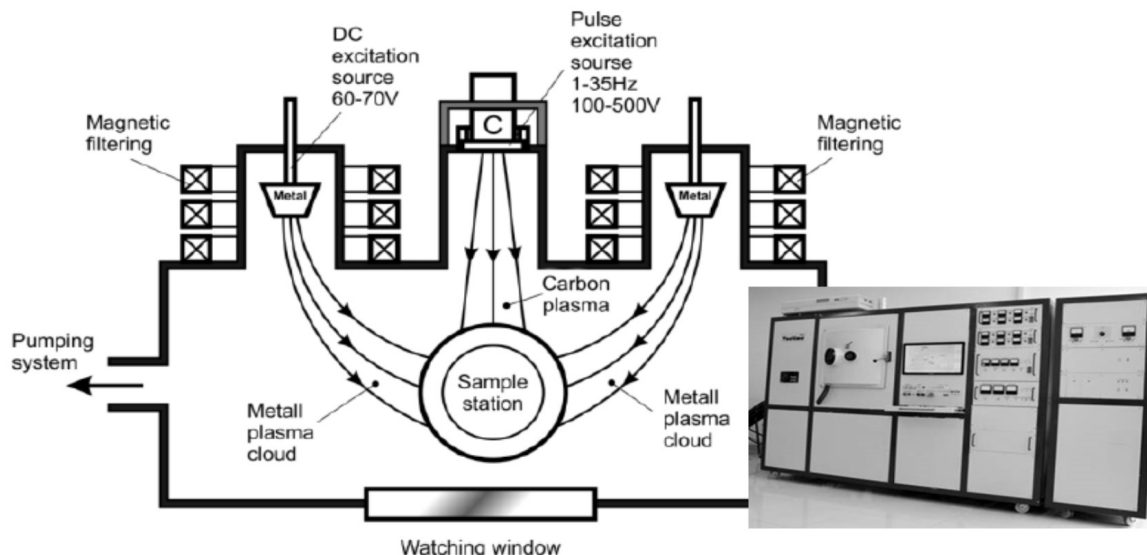
---

*Corresponding author. E-mail: pdg_@mail.ru

Fig. 1. Schematic diagram of film deposition device with double-excitation cathode arc source.

The polished stainless steel (304) and n-type silicon (100) wafers were used as substrates. They were cleaned ultrasonically in acetone and ethyl alcohol at about 50 °C for 15 min and then dried in air. The chamber was cleaned with Ar for 3 min at $6 \times 10^{-4}$ Pa to get rid of residual air. Prior to deposition, the substrates were cleaned for 15 min using Ar$^+$ sputtering under the discharge current of 3 A and the voltage of 350 V. A metallic Cr target of 99.5% purity was DC cathode evaporated for preparing Cr-interlayer.

A graphite target of 99.5% purity was pulsed arc cathode evaporated for obtaining DLC films. To reduce the impact of the substrate temperature on the film deposition process, the films were cooled in vacuum to room temperature after their ion cleaning. During film deposition, the rotation velocity of the sample holder was kept at 2 rev/min.

DC arc current for Cr target, pulse frequency, pulse number of pulse carbon source were 60A, 10 Hz and 4500, respectively. The thickness of Cr layer were changed by time of evaporation Cr cathode with DC arc. Then, by controlling the deposition time of Cr layer, we can prepare the films with different thickness of Cr layer and parameters of deposition process are shown in Table 1.

The film thickness was measured by a 3D optical profiler (Ambios Technology XP-2).

The bonding state of carbon was analyzed using a Renishaw in Via (England) Raman spectrometer, with an Ar$^+$ laser operating with a power of 20 mW. The deconvolution of the peaks was executed by curve fitting using Gaussian-Lorentz function with a Gaussian fraction of 20%. Surface morphology and roughness (RMS) were tested by the Dimension Icon (Bruker) atomic force microscope (AFM) in tapping mode with a scanning scope of $10 \times 10$ µm$^2$ and a scan rate of 1.0 µm/s.

The internal stress of the amorphous DLC film are the important factors to determine the properties of the films. The film wear parameters depend on the high internal stress, which make deformation and crack, greatly reduce the applications of the film, therefore, the analysis of internal stress and adhesion in thin films is extremely important.

As reported in [6, 7], residual stress $\sigma$ in the films is composed of three major components: thermal stress $\sigma_t$, intrinsic stress $\sigma_i$ and extrinsic stress $\sigma_e$, as shown in Equation $\sigma = \sigma_t + \sigma_i + \sigma_e$. Thermal stress is mainly caused by two reasons: the first is resulted from the difference in thermal expansion coefficients of a deposited film and substrate [8], the second is the film deposited at very high temperature. In our case, the films were deposited at room temperature and, therefore, the thermal stress is negligible. The internal stress is caused by different deposition process conditions [9]. The intrinsic stress in the films is directly dependent on the deposition rate, ion energy, deposition temperature and residual atmosphere in the chamber, and thus all these parameters were optimized during the sample manufacture based on our previous experience [6, 11]. The extrinsic stress is caused by external factors after the film deposition, for example, induced by the reactions of oxygen impurity with C and Cr atoms or absorbance the polar molecules from the atmosphere. Excessive residual stresses in the films may cause the formation of defects and the delamination of the film-substrate interface. Therefore, it is necessary to analyze the impact of the structure and composition of the films on the level of residual stresses [10].

**Table 1**
Compare result of deposition parameters vs thickness and results of mathematical fitting of Raman spectra

| Samples name | Pulse carbon frequency, Hz | Number of pulses | DLC thickness, nm | Deposition time of Cr layer, min | Cr thickness, nm | G peak width, cm$^{-1}$ | G peak positions, cm$^{-1}$ | $I_D/I_G$ ratio |
|---|---|---|---|---|---|---|---|---|
| DLC | 10 | 4500 | 217 | 0 | 0 | 211.4 | 1562.3 | 0.17 |
| Cr$_{28nm}$/DLC | 10 | 4500 | 220 | 3 | 28 | 236.6 | 1562.2 | 0.19 |
| Cr$_{43nm}$/DLC | 10 | 4500 | 218 | 5 | 43 | 228.0 | 1578.0 | 0.40 |
| Cr$_{57nm}$/DLC | 10 | 4500 | 230 | 7 | 57 | 237.9 | 1567.0 | 0.36 |

According to the Stoney formula, $\sigma = \frac{1}{6R} \frac{E_s}{1-y_s} \frac{t_s^2}{t_f}$, the residual stress ($\sigma$) in the films was determined by the change in curvature radius of the Si substrate before and after the films deposition using a stylus profiler (Dektak XT, Bruker). Here $E_s = 146$ GPa, $\gamma_s = 0.266$, $t_s = 0.5$ mm are Young's modulus, Poisson ratio and thickness of substrates, respectively. Both the radius of curvature $R$ and the film thickness $t_f$ are also measured by the stylus profiler.

Microhardness of the film can be used to measure the ability of the film to resist of deformation, the hardness value is easy to be affected by the thickness of the film and the substrate material. The microhardness (Hk) of the films was measured by an AFFRI DM-8 Knoop sclerometer. Polished silicon wafers were used when measuring microhardness. A rhombic pyramid diamond indenter was set at the angle of 172°30' between the long edges of the pyramid. The test conditions are 0.3 mN and 10 s, respectively. The hardness of each sample is measured at 10 points, and the average value of each sample is the hardness of the film. The thickness of the film is small and the measured hardness and elastic modulus of film are the composite hardness of film-substrate system, be noted that the measurement results only for the qualitative comparison, does not reflect the film's hardness and elastic modulus.

DLC film has good resistance to friction and wear, the friction coefficient and wear rate is affected by the physical and chemical compositions of the DLC film and preparation technology. The test conditions are affected to the friction coefficient range from 0.001 to 0.6. The factors of wear of the DLC films were divided into intrinsic and external factors. Intrinsic factors of the friction of DLC films is depends on sp$^3$ and sp$^2$ bond ratio, the availability of doping element, surface topography and roughness. External factors mainly refer to the test conditions (load and counterbody materials, friction velocity), test environment (temperature, humidity, atmosphere) and medium (water, oil, corrosive liquids), by changing the physical and chemical states of the interface friction and affect the tribological properties of the films. In this paper, the tribological properties of the films are almost the same, so the influence of the external factors can be neglected. UMT2-EC type friction and wear testing machine produced by Bruker company was used to test the friction coefficient of thin film, load is 0.5 kg, sliding speed is 8 mm, duration time is 3000 s, friction couple was Si$_3$N$_4$ ball with diameter of 3 mm/s. Test room temperature is 18 ~ 21, the relative humidity of RH is 45 ~ 50%. The tribological properties of DLC thin films were evaluated by the comparison of the surface profile after the friction loss.

DLC film has high resistivity and chemical inertness which make it practically insoluble in any acid, base or organic solution, it can be used as a protective film to inhibit the penetration of oxygen and solutions to protect the base material from corrosion [6]. The wetting properties of the film reflect the ability of suppressing penetration of the solution to a certain extent. Therefore, it is necessary to study the wetting properties and corrosion resistance. The wetting properties reflect the surface properties of the films, the contact angle of the common solid surface is measured, and it affected by the composition, structure and surface morphology. A certain volume of liquid put on the films surface, when the liquid droplet is balanced, the included angle of the interface between the solid liquid and the liquid gas is measured (is called the contact angle). In this paper, SL200KB work station were used to test the contact angle. Test was done the sessile drop method at room temperature, each film surface titration saline solution 5 μl of each sample six different random measurement points, the average value as the value of the contact angle of the surface of the film.

Amorphous DLC film have a high resistivity and density, which can effectively prevent the deepening of the ions in the liquid corrosion. As know that corrosion mainly rests on the surface of the film, but in the deposition of thin film, due to the preparation process, there are some defects on the surface of the film, such as pinhole, gap, weak interface, etc., which decrease corrosion resistance performance.

The method of evaluating the corrosion resistance of DLC thin film is many, among which the electrochemical method is simple, easy to operate, good repetition and high sensitivity.

Corrosion resistance of Cr/DLC films was evaluate by potentiodynamic polarization using electrochemical workstation. A three standard electrode system in artificial seawater was used to test potentiodynamic polarization. A Pt sheet and a saturated calomel electrode (SCE) were used as counter and reference electrodes, respectively. Potential ranged from – 2 and 2 V at a scanning rate of 5 mV/s. The corrosion morphology observed by metallographic microscope shows in the form of three-dimensional graphs [6].

## 3. Results and discussion

Figure 2 shows Raman spectra of the Cr/DLC r films with different thickness of Cr layer. All spectra show a broad peak with symmetry in the range of 1100–1800 cm$^{-1}$, centered at 1570 cm$^{-1}$, revealing the presence of sp$^2$- and sp$^3$-hybridized bonding carbon and high disordering in the films.

For the Cr/DLC films, the form of the broad peak has no shows change with the thickness of Cr layer, but the peak intensity corresponding to the quantity of carbon–carbon bonds varies with the thickness. Note that the intensity of the Raman peak increases monochromatically with increasing the Cr layer thickness, which indicated that a thickness of Cr layer would induce the decrease of carbon–carbon (sp$^2$ or sp$^3$) bonds as a result of high diffusion between Cr and carbon layers [11].

The variation in the intensity ratio of the D peak to the G peak ($I_D/I_G$) and the position and width of the G peak can give some information on the ordering and amount and size of sp$^2$-bonding carbon in the DLC films.
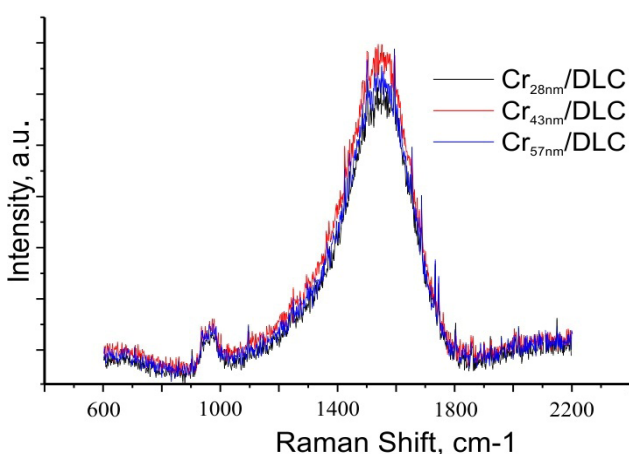


Fig. 2 Raman spectra of Cr/DLC thin films with different thickness of Cr layer.

Table 1 shows the results of mathematical fitting of Raman spectra for Cr/DLC films with different thickness of Cr layer.

As can be seen from Table 1, the $I_D/I_G$ ratio of increases and the G-peak width increases with increasing the thickness of Cr layers in the film from 28 to 57 nm.

When DLC layer was deposited from above Cr layer, independently of the Cr thickness, the G peak width and $I_D/I_G$ ratio increases in compare with DLC monolayer.

For a thinner Cr interlayer (28 nm) the $I_D/I_G$ ratio has no significant variation, indicating the size of sp$^2$-bonding carbon clusters the same like pure DLC.

For Cr/DLC film with Cr thickness above 28 nm, $I_D/I_G$ ratio indicates the decrease of the size and quantity of sp$^2$-bonding carbon clusters, which is a result of the reduction of carbon – carbon bonds and the formation of CrC phase. The observations on the position and width of the G peak also demonstrate the microstructure evolution induced by the reaction of Cr with C atoms.

Meanwhile, the G peak position increases, and the G peak width increases with Cr layer thickness increases from 20 to 45 nm, implying more disordering of sp$^2$-bonding carbon clusters. These results demonstrate the growing and disordering of sp$^2$-bonding carbon clusters for the Cr/DLC films, attributing influences the defects of surface structures of Cr layer on the growth of amorphous carbon layer.

At show in SEM image (Fig. 3) Cr$_{28nm}$/DLC and Cr$_{57nm}$/DLC films appears in the film surface is more smooth, barely noticeable particles, but the surface Cr$_{43nm}$/DLC film has larger particles. HRSEM images (under the 500 nm resolution), was shown that all the film surface appears particulate matter, the film surface Cr$_{28nm}$/DLC and Cr$_{57nm}$/DLC less than the surface of the film particles. Typically, the film surface particles less, the smoother surface, the surface roughness is. Thus, SEM analysis chart pattern analysis consistent with AFM match.

Figure 4 shows the topography and phase contrast images of Cr/DLC films with different Cr thickness.

It is observed that Cr$_{28nm}$/DLC films shows smooth and amorphous surface morphology, and when the Cr layer thickness increases, more graphitic particles with large size are produced on the film surface. These particles may be graphitic carbon aggregations from phase contrast images.

From the Fig. 4, there are a lot of large grain of surface of Cr$_{43nm}$/DLC thin film. Based on the analysis of surface roughness, the root mean square roughness (RMS) of Cr$_{43nm}$/DLC films is about
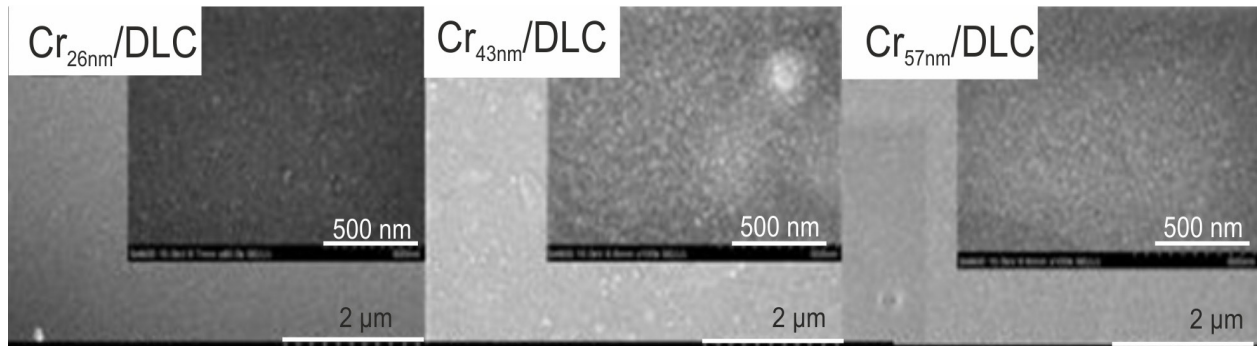
Fig. 3. SEM of DLC thin films with different thickness of Cr transition layer.

87.67 nm, and its bigger than the RMS of $Cr_{28nm}$/DLC and $Cr_{57nm}$/DLC films, which have a $R_{MS}$ 21.26 nm and 23.84 nm respectively.

It can be seen from Table 2, that the hardness of the Cr/DLC films decreases when the thickness of Cr layer become to 28 nm, and increase when thickness of Cr layer become to 43 nm, which may be attributed to the formation of hard carbide phase. When the thickness of Cr layer increases to 57, the hardness of the film decreases. These indicate that the decrease of the hardness for the $Cr_{57nm}$/DLC film is a result of the effect of soft metal layer.

As the Table 2 shows, internal stress of three Cr/DLC thin film samples with Cr transition layer was lower than the internal stress of DLC films. This is because Cr transition layer can reduce film – substrate physical properties caused by the difference of lattice and thermal mismatch, so the stress of films low. But some difference in $Cr_{43nm}$/DLC film and $Cr_{57nm}$/DLC film internal stress. According to it, we may infer the stress changes and not has been subsequently transition layer thickness increased

and decreased, it should be of the existence of the limit thickness. When the thickness of the transition layer reaches the thickness can ignore the influence of substrate on the properties of the films. The minimum stress of $Cr_{28nm}$/DLC thin film is only 0.38 GPa, which shows that the Cr transition layer prepared under this process has the best effect on reducing the internal stress of the film.

Because the surface roughness of $Cr_{28nm}$/DLC and $Cr_{57nm}$/DLC films is similar, the coefficient of friction is close to that of, and it is obviously smaller than the friction coefficient of DLC film, which indicates that the design of Cr transition layer can reduce the friction coefficient of the DLC film to a certain extent. $Cr_{43nm}$/DLC friction coefficient is slightly larger than the friction coefficient of DLC films, but taking into account the existed on the surface of individual large particles, causing the surface roughness is larger, which may is preparation process issues caused by instability here is not suitable for evaluating the quality of the friction coefficient.
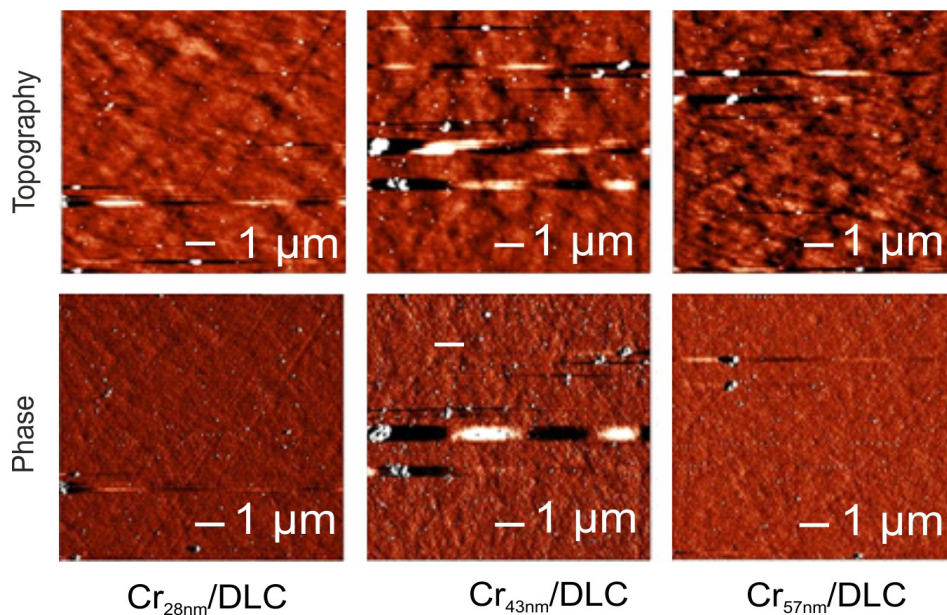


Fig. 4. AFM of DLC thin films with different thickness of Cr transition layer.

**Table 2**
The mechanical properties of Cr/DLC films with different Cr thickness parameters

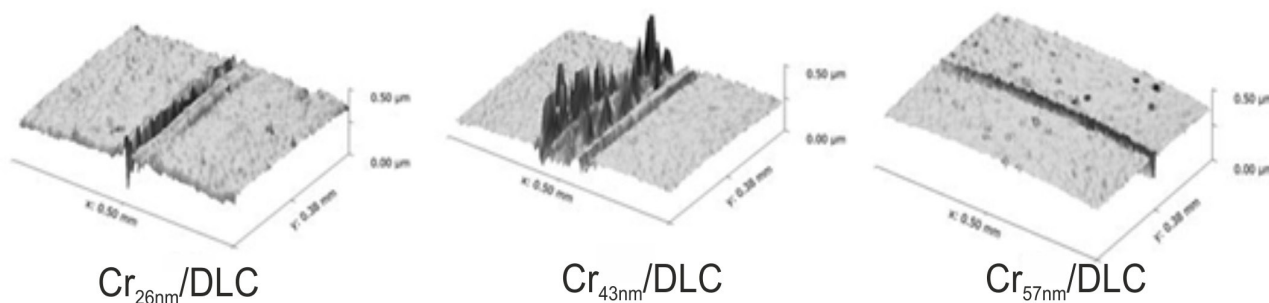| Samples name | Internal stress, GPa | Friction coefficient, μ | Microhardness Hk, GPa | Elastic Modulus, GPa |
|---|---|---|---|---|
| DLC | 0.53 | 0.17 | 14.3 | 384.95 |
| Cr$_{28nm}$/DLC | 0.38 | 0.12 | 13.8 | 403.42 |
| Cr$_{43nm}$/DLC | 0.49 | 0.21 | 16.8 | 406.46 |
| Cr$_{57nm}$/DLC | 0.48 | 0.10 | 11.3 | 398.37 |



Fig. 5. 3D views of a typical wear track for DLC thin films with different thickness of Cr transition layer.

The hardness and elastic modulus of Cr$_{28nm}$/DLC, Cr$_{43nm}$/DLC and Cr$_{57nm}$/DLC thin films are larger than that of DLC thin films. According to Raman spectroscopy, Cr transition layer has a certain influence on the microstructure of DLC films, content of carbon bonds in films determines hardness and elastic modulus of DLC film, but Cr interlayer thickness also have a certain influence on the film hardness and elastic modulus. So, although the content of sp$^3$ hybrid bonds in Cr$_{43nm}$/DLC thin films is low, it has strong hardness and high elastic modulus, that, in our opinion, is connected with the formation of diffusion carbide layer [12, 13].

3D images of the friction tracks shown in Fig. 5. Cr$_{28nm}$/DLC and Cr$_{57nm}$/DLC show the highest depth of the track and confirm abrasive wear of the films for which microcutting of the surfaces is typical. But surface of Cr$_{43nm}$/DLC films have projections which can destroy the surface of counterbody during friction. 43 nm/DLC films have more sp$^2$ bond in the film structure, but surface roughness is larger, so in the friction process, particles on the friction surface is work like the abrasive grains in the contact friction track and increase the wear process, due to this is the destruction of the film. The particles of Cr$_{28nm}$/DLC and Cr$_{57nm}$/DLC films are less, and the surface roughness is relatively low. Among them, because the Cr transition layer of Z3 thin film is thicker, the friction performance of the film is greatly reduced, so the friction and wear resistance is the best [14].

The contact angles Θ° of Cr/DLC thin films with different thickness of Cr layer are shown in Fig. 6.

The Θ° sorted in descending order is Cr$_{28nm}$/DLC, Cr$_{43nm}$/DLC, Cr$_{57nm}$/DLC, corresponding value is 62.28º, 70.34º, 72.42º, respectively. Usually, if the film Θ° is larger than 90° then it is hydrophobic, and if its Θ° is lower than 90° then it is hydrophilic. Cr/DLC films with different Cr thickness show the contact angle Θ° of less than 90º, so the film has a hydrophilic.

The corrosion properties of the samples are performed in an artificial seawater solution to investigate the protective abilities of films. The corrosion parameters for all the samples are shown in Fig. 7 and Table 3.

**Table 3**
The corrosion parameters of Cr/DLC films with different Cr thickness

| Samples name | E$_{corr}$, V | I$_{corr}$, μA | V$_{corr}$, μA/cm$^2$ |
|---|---|---|---|
| DLC | -1.32 | 37.8 | 31.7 |
| Cr$_{28nm}$/DLC | -0.88 | 32.75 | 32.75 |
| Cr$_{43nm}$/DLC | -0.38 | 39.96 | 32.02 |
| Cr$_{57nm}$/DLC | -0.51 | 32.02 | 39.96 |



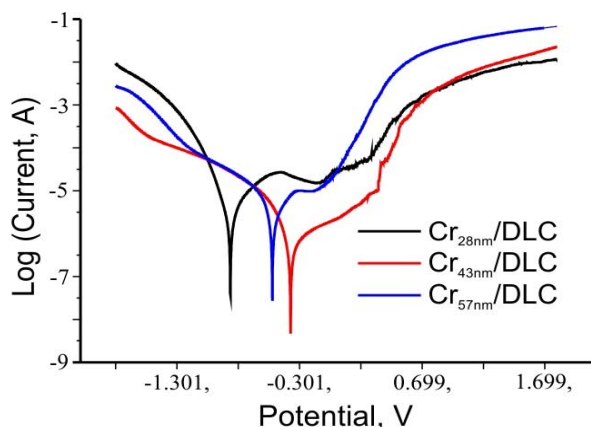Fig. 6. The contact angles of Cr/DLC thin films with different thickness of Cr layer.

Fig. 7. Tafel polarization curves of Cr/DLC thin films with different thickness of Cr layer.

Usually, the smaller the corrosion potential, the easier the film is prone to corrosion [6, 15], so $Cr_{43nm}$/DLC film has better corrosion resistance performance, and the corrosion resistance of $Cr_{28nm}$/DLC film is worse. Besides, major contribution of $sp^2$ hybrid bonds in the $Cr_{43nm}$/DLC film structure that is known from the analysis results of Fig. 2 and Table 1 can promote electron transference and exchange, leading to greater corrosion. On the contrary, the lower $sp^2$ hybrid bond content, the better corrosion resistance. Chromium carbides are formed from chemical interactions between chromium and carbon atoms in its structure, which can slow down the corrosion or, in other worlds, to facilitate anti-corrosion.

## 4. Conclusion

Cr/DLC films with different chromium thickness are produced by the cathode arc plasma technique. The effect of the Cr thickness on microstructure, morphology, and properties of Cr/DLC films are studied. A detailed comparative analysis of structural, corrosive and mechanical properties of the Cr-modified two layer a-C films is made. According to this analysis, we can conclude that the Cr-underlayer can substantially change the content of $sp^3$ hybridized carbon atoms in the structure and the degree of ordering of $sp^2$-C clusters due to Cr bonding with carbon atoms. The combination of Cr-interlayer and Carbon layers can considerably change the microhardness and residual stress, improve wear resistance. The films with the Cr-interlayer of 28 nm show the best integrated results in residual stress and microhardness, but also corrosion-resistance characteristics. There is no doubt, that these advanced characteristics are in high demand for those industries dealing with production of ruggedized parts.

## Acknowledgements

## Reference

[1]. N. Dwivedi, S. Kumar, H.K. Malik, C.M.S. Rauthan, O.S. Panwar, Plasma Processes & Polymers 8 (2) (2011) 100–107.

[2]. T. Horiuchi, K. Yoshida, T. Okuda, et al. Surf. Coat. Technol. 205 (7) (2010) S188–S95.

[3]. P. Písařík, M. Jelínek, K. Smetana, et al. Appl. Phys. A 112 (1) (2013) 143–1488.

[4]. G. Ma, S. Gong, G. Lin, L. Zhang, and G. Sun. Appl. Surf. Sci. 258 (7) (2012) 3045–3050.

[5]. X. Li, P. Ke, A. Wang, J. Phys. Chem. C 119 (11) (2015) 6086–6093.

[6]. Y. Zhuang, X. Jiang, A.V. Rogachev, D.G. Piliptsou, B. Ye, G. Liu, T. Zhou, A.S. Rudenkov, Appl. Surf. Sci. 351 (2015) 1197–1203.

[7]. Wang, X. Wang, T. Xu, W. Liu, J. Zhang, Thin Solid Films 515 (2007) 6899–6903.

[8]. S.K. Pal, J. Jiang, E.I. Meletis, Surf. Coat. Technol. 201 (18) (2007) 7917–7923.

[9]. K Azuma, E Fujiwara, M. Yatsuzuka, Surf. Coat. Technol. 186 (1) (2004) 141–145.

[10]. E. Mounier, Y. Pauleau, Diamond Relat. Mater., 6 (9) (1997) 1182–1191.

[11]. B. Zhou, A.V. Rogachev, Z. Liu, et al. Surf. Coat. Technol. 208 (6) (2012) 101–108.

[12]. W.C. Oliver, C.J. Mchargue, Thin Solid Films 161 (7) (1988) 117–122.

[13]. A.M. Korsunsky, A. Constantinescu, Mater. Sci. Eng., A 423 (s 1–2) (2006) 28–35.

[14]. A. Pardo, J.G. Buijnsters, J.L. Endrino, C. Gómez-Aleixandre, G. Abrasonis, R. Bonet, J. Caro, Appl. Surf. Sci. 280 (2013) 791–798.

[15]. R. Hatada, S. Flege, A. Bobrich, W. Ensinger, K. Baba, Surf. Coat. Technol. 256 (2014) 23–29.